# The effect of wall thermal inertia on the stability of a natural circulation driven supercritical water reactor

K.W.W. Kewal

Bachelor of Science Thesis

Delft University of Technology
Faculty of Applied Sciences
Dept. of Radiation Science and Technology
Sect. Nuclear Energy and Radiation Applications

**Supervisor:** Dr.ir. M. Rohde

**Committee:** Dr.ir. M. Rohde, TNW, TU Delft
**Committee:** Dr. ir. D. Lathouwers, TNW, TU Delft

Delft, 27 June 2016

# Abstract

The supercritical water reactor(SCWR) is a reactor that operates under high pressure and high temperature in the supercritical state. In the reactor core the density drops greatly from 780 to 90 kg/m$^3$, which makes the SCWR suitable for natural circulation driven designs. The high performance light water reactor(HPLWR) is the european design for an SCWR.

The Delft light water reactor (DeLight) was built at the TU Delft, as a scaled experiment of the HPLWR. T'Joen and Rohde (2012) experimentally determined the stability of the HPLWR. Previous studies using a numerical code have shown that thermal inertia in the core had a large effect on the stability of the DeLight model.

In this thesis the effect of thermal inertia in the riser wall on the stability of the HPLWR has been numerically researched. It was found that adding riser thermal inertia increased the stability in the type II density wave oscillations. The amount of thermal inertia was increased by increasing the wall thickness. The system was found to become more stable as the riser wall thickness is increased from $10^{-15}$ until 0.1 mm and then destabilize when the thickness is further increased to 50 mm. At a thickness of 100 mm the system was found to be very stable. No explanation has been found for the local minimum and maximum in the stability.

Lastly a correction has been made to the model for natural convection from the core to the environment. This had a stabilizing effect on the system. The resulting stability boundary closely resembles the experimental results for low and medium $N_{PCH}$.

# Contents

# Chapter 1

# Introduction

## 1.1 Supercritical water reactors

The supercritical water reactor (SCWR) is a type of generation IV reactor design that utilizes light water under high pressure, that is heated in the core to the supercritical state. The supercritical state occurs at a pressure and temperature than the critical temperature and critical pressure of the water. In this region there is no separate gas phase. The advantage of this is that the water can be heater to a much higher temperature than in a boiling water reactor (BWR), because the outlet temperature is no longer limited to the boiling point. This higher operating temperature results in a maximum thermal efficiency of 45% compared to the 33% in a BWR.

The SCWR operates on a temperature range of 280 – 500 °C and at a pressure of 25 MPa. During the heating process in the core, the water density drops from 780 kg/m$^3$ to 90 kg/m$^3$ (Ortega Gómez, 2009). This makes a SCWR extremely suitable for a natural circulation driven design. In this thesis only the natural circulation driven design is considered.

The SCWR utilizes a once-through coolant cycle, similar to those used in fossil boilers (Tsiklauri et al., 2005). The reactor heats the water in the core, and then it flows through a turbine and condenser, where it is cooled down to the inlet temperature and flows into the core again.

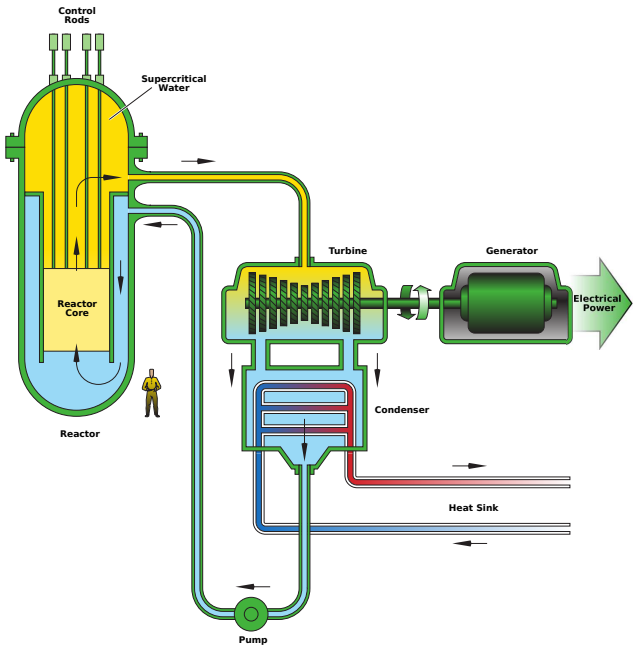


**Figure 1.1:** Schematic overview of the SCWR design utilizing the once-through cooling cycle.The reactor heats the water in the core, and then it flows through a turbine and condenser, where it is cooled down to the inlet temperature and flows into the core again. Note that this thesis only considers a natural circulation driven SCWR, ie. without pump.

## 1.2 High performance light water reactor

The high performance light water reactor (HPLWR) is the European design for the SCWR. It consists of a three-pass core, where the water is heated in stages with mixing chambers in between the core sections. This is shown in figure 1.2. The mixing chambers serve to homogenize the water temperature in the channel and prevent local hot spots in temperature that could exceed the cladding temperature limit (Ortega Gómez, 2009). The three heated core sections are respectively called the evaporator, superheater I and superheater II. The evaporator heats the water past the pseudocritical temperature, under a subcritical pressure this would evaporate the water, hence its name, even though technically no evaporation occurs. The superheaters further heat the supercritical water up to 500°C.

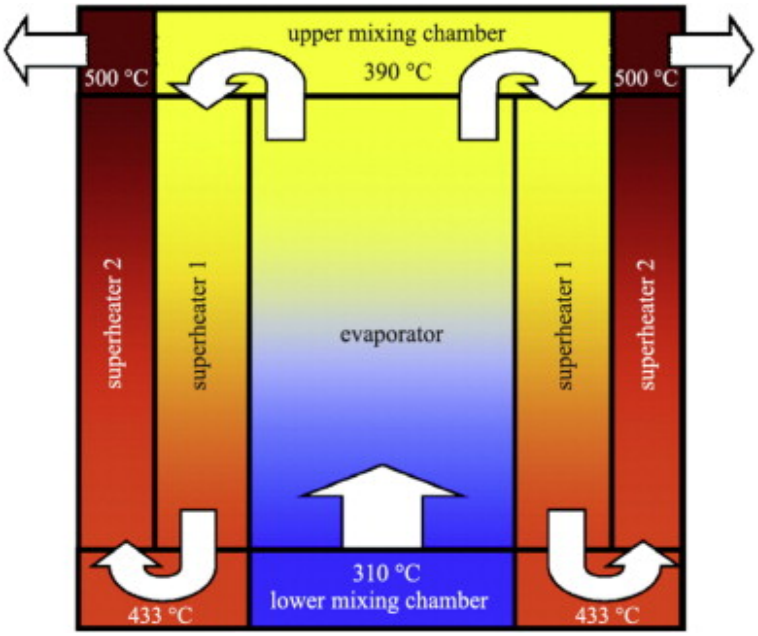


**Figure 1.2:** Schematic overview of the three-pass core design with mixing chambers in-between the core sections (Schulenberg, Starflinger, & Heinecke, 2008).

Water in the HPLWR acts as both a coolant as moderator. The moderation is heavily dependent on density of the water. A lower density means less moderation, which lowers the core power. This causes the temperature to drop and density to increase again.

## 1.3 Literature survey

In 2012 T'Joen and Rohde (2012) conducted an experimental study to simulate the stability of the supercritical water reactor. The experiments were conducted in a facility called Delft Light Water Reactor, or DeLight for short. The DeLight facility was a scaled version of the HPLWR, that utilized Freon R-23 as scaling fluid. The result was a Neutral stability boundary (NSB) in a dimensionless plane of pseudo phase change number ($N_{PCH}$) and a subcooling number ($N_{SUB}$). $N_{PCH}$ can be seen as the enthalpy gained in the core and $N_{SUB}$ can be interpreted as the inlet temperature, where high inlet temperature gives a low $N_{SUB}$.

Later, in 2012, Spoelstra (2012) wrote a 1D numerical model to simulate the DeLight experiments. This numerical code was based on a model by Kam (2011), who adjusted the STEALTH model for natural circulation driven BWRs (Koopman, 2008) for use on supercritical conditions. The NSB found by Spoelstra (2012) agreed with T'Joen and Rohde (2012) for low $N_{PCH}$, but predicted a much larger instability for high $N_{PCH}$. This was due to several assumptions made. There was no thermal inertia from the core and riser, and the heat flux in the core was uniform throughout each core section. Natural convection was simulated as a constant percentage of the core power. Furthermore heat transfer correlations for subcritical flows were used.

Schenderling (2013) implemented a model for thermal inertia in the heated core sections and natural convection to the environment. It was shown that these models greatly increased the stability of of the

system, however there was still a large discrepancy with he experimental results.

Van Iersel (2016) built upon the improvements by Schenderling (2013) and examined different friction and Nusselt relations for forced convection to supercritical flows. The resulting NSB was less stable than the one found by Schenderling (2013), but resembled the experimental results more closely.

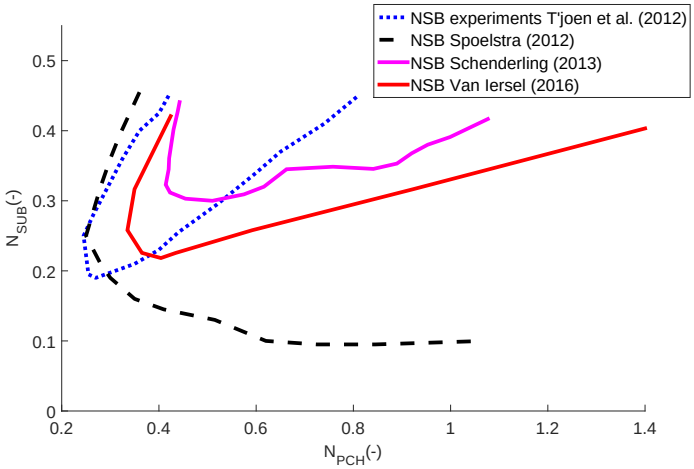


**Figure 1.3:** The Neutral stability boundary in the dimensionless plane as experimentally found by T'Joen and Rohde (2012) and numerical boundaries as found by Spoelstra (2012), Schenderling (2013) and Van Iersel (2016). The dimensionless number $N_{PCH}$ and $N_{SUB}$ represent different operating points of the DeLight facility. Source: Van Iersel (2016)

Figure 1.3 shows the different NSBs found by T'Joen and Rohde (2012), Spoelstra (2012), Schenderling (2013) and Van Iersel (2016). It can be seen that none of the models accurately mimic the experimental results. This could be due to several assumptions still present in the model by Van Iersel (2016): there is no thermal inertia modeled in the riser and the heat exchanger and downcomer are modeled in a non physical way.

## 1.4 Thesis objectives and outline

This thesis has the objective to study the effect of thermal inertia in the riser wall on the stability of the DeLight facility. This thesis will be a continuation of the work done by Van Iersel (2016), Schenderling (2013) and Spoelstra (2012).

First a model for thermal inertia will be implemented in the riser. This model will be validated by comparing it to the NSB by Van Iersel (2016). Afterwards the amount of thermal inertia is varied to study the effect of thermal inertia on the stability of the DeLight facility. Finally a correction will be made on the natural convection model by Schenderling (2013) and its effect will be analyzed.

The outline of this thesis is as follows: after this introduction, the theory required to understand this work will be discussed in a general way in chapter 2. Chapter 3 gives an overview of the DeLight facility, its geometry and its components. Chapter 4 will introduce the numerical DeLight model and explain the implementation of the inertia and natural convection models. Chapter 5 discusses the experimental methods used to obtain steady state results from the DeLight model, how the stability is analyzed and how the code is validated against the results by Van Iersel (2016). Chapter 6 shows the results of the implementation of the inertial and natural convection model and discusses these. Finally in chapter 7 consists of the conclusions and outlook.

# Chapter 2

# Theory

## 2.1 Supercritical fluids

A fluid under high pressure has an increased boiling point. At a certain pressure there is no longer a transition from liquid to gas-phase. Figure 2.1 shows the phase diagram for water. At the end of the boiling line is the so-called critical point, with a critical temperature ($T_c$) and a critical pressure ($\mathcal{P}_c$). For pressures and temperatures higher than the critical point the fluid is in the supercritical state. For water the critical point is at $T_c = 374.2°\text{C}$ and $\mathcal{P}_c = 22.1$ MPa.

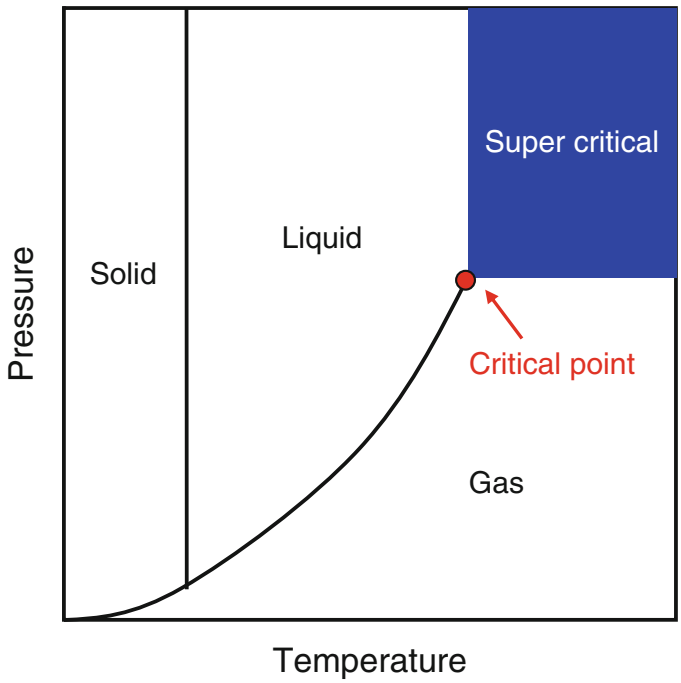


**Figure 2.1:** Phase diagram with supercritical region at higher pressures and temperatures than the critical point (Oka, Koshizuka, Ishiwatari, & Yamaji, 2010)

At a subcritical pressure the thermal-physical properties of the fluid, e.g. density, viscosity and specific heat, change abruptly during the phase transition. In the supercritical phase there is a pseudocritical point where the fluid changes in a similar way from a liquid-like state to a gas-like state. It however still remains a liquid.

The pseudocritical point is defined as follows(Pioro & Mokry, 2011): a point at a pressure above the critical pressure and at a temperature corresponding to the maximum value of the specific heat at this particular pressure.

The pseudocritical point can be found by extrapolating the vaporization line in the phase diagram. At the pseudocritical point the supercritical fluid properties also change (Oka, Koshizuka, Ishiwatari, & Yamaji, 2010). This change is continuous, as opposed to the discontinuous change in subcritical properties. This difference is shown in figure 2.2. Figure 2.3 shows the change in properties for water in the HPLWR temperature range between 280 – 500 °C.

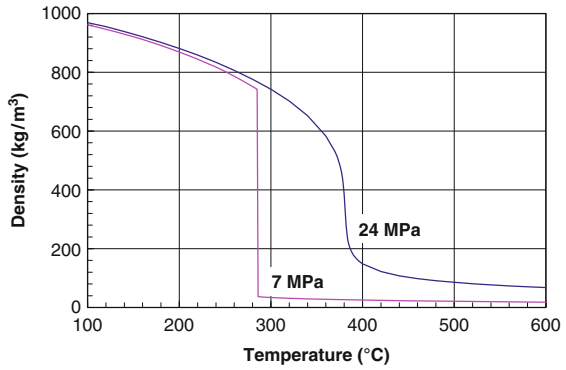


**Figure 2.2:** Change in density for subcritical (7 MPa) and supercritical(25 MPa) water. The subcritical water shows a discontinuity, while the supercritical pseudo phase change is continuous. (Oka, Koshizuka, Ishiwatari, & Yamaji, 2010).

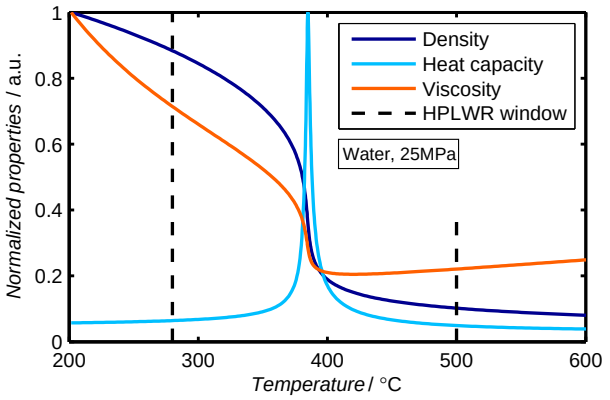


**Figure 2.3:** Normalized properties of water in the operating window of the HPLWR at 25 MPa. A sudden change in properties can be observed at the pseudocritical temperature (Spoelstra, 2012).

At higher pressures the change in thermal-physical properties becomes more gradual (Squarer et al., 2003). It should also be noted that at higher pressures the pseudocritical point occurs at a higher temperature. This is shown in figures 2.4(a) and 2.4(b). Here the pseudo-phase change occurs at a higher temperature and becomes more gradual.

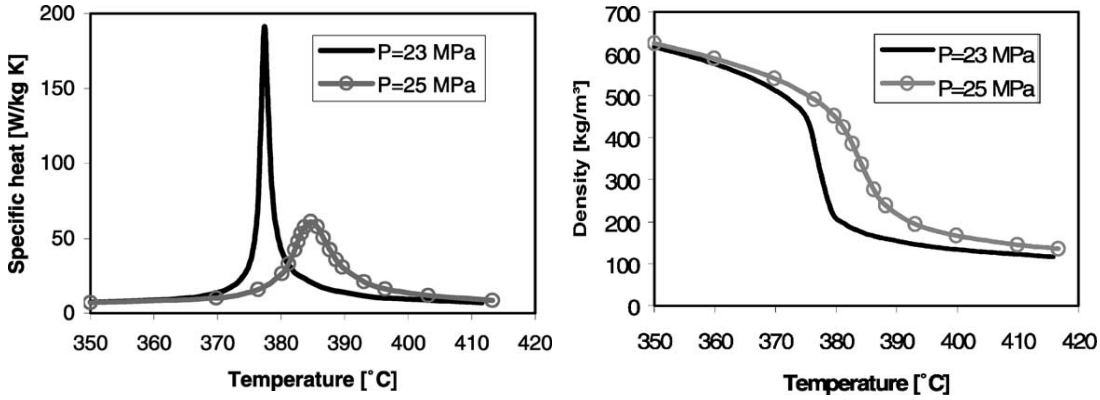


(a) The change in specific heat around the pseudocritical temperature.

(b) The change in density around the pseudocritical temperature.

**Figure 2.4:** At higher pressure the change in thermal-physical properties around the pseudocritical properties becomes more gradual (Squarer et al., 2003). Note that the pseudocritical point occurs at a higher temperature for higher pressures.

## 2.2 Stability of natural circulation driven supercritical water reactors

A system's stability is determined by its response to a perturbation on one of the system parameters. The are various kinds of instabilities, which can be divided in two main categories: static instabilities and dynamic instabilities (Bouré, Bergles, & Tong, 1973).

Static instabilities can be described using steady state equations. When the flow conditions are slightly perturbed, static instabilities occur if another steady state is not possible near the original one. Dynamic

instabilities occur when inertia and feedback effect are in play. To study dynamic instabilities, one needs the needs to know the transient behavior of the system.

In the following subsections a few different instabilities are discussed: Ledinegg instabilities, boiling crisis and density wave oscillations.

### 2.2.1 Ledinegg instabilities

A Ledinegg instability, also known as flow excursion, is a sudden change in flow rate to a lower value (Ledinegg, 1938). This instability is static and non-periodic. It occurs when multiple steady flow states are possible in the system. A small perturbation can then cause the flow to move between different steady states. When the system moves to a steady state with a slower flow rate, this may induce a boiling crisis, this is discussed in the next subsection.

### 2.2.2 Boiling crisis

A boiling crisis is a general term used to describe the deterioration in the heat transfer rate. Although supercritical water technically does not boil, its properties still change past its pseudocritical temperature, where the water transitions from liquid-like to gas-like state. Under a high heat flux and low flow rate heat transfer deterioration occurs, similarly as if the water was subcritical. The water at the wall will 'boil', creating a thin film of supercritical water in the gas-like state, this is called thin film boiling. The gas-like supercritical water absorbs less heat from the wall and as consequence the wall temperature excursions occur, which can cause flow oscillation(Boure, Bergles, & Tong, 1973).

### 2.2.3 Density wave oscillations

Pressure drop oscillations (DWO) are a dynamic instabilities caused by feedback effect relating the flow rate, density and pressure drop. DWOs are the most common type of instability in a BWR, due to large density differences in a BWR. Since this is also the case in a SCWR, it is expected that DWOs will also occur in the SCWR.

DWOs are caused by a fluctuation in e.g. the mass flow. When this fluctuation moves through the core, the regions with a low mass flow will stay longer in the core than the regions with a high mass flow, which causes the low mass flow regions to get hotter and less than high mass flow regions. This results in a sinusoidal density profiles in the system.

There are three types of DWOs respectively called type I, type II and type III. Type I DWOs are caused by gravitational pressure drops. These are found in upward vertical systems with long unheated riser sections (Ruspini, 2013). This type of instability plays an important role in natural circulation driven system (Collins & Gacesa, 1969). When the core outlet temperature is near the pseudocritical temperature, DWOs are created. These Oscillations cause an oscillation in the gravitational pressure drop. When these pressure drop oscillations are out of phase with the density waves, positive feedback can occur.

Type II DWOs are similar to Type I DWOs, except caused by frictional pressure drops. The friction in the tube is dependent on the flow speed(Fang, Xu, Su, & Shi, 2012). A perturbation in the flow speed can cause an oscillation in the friction, which causes a oscillation in the pressure drop. When the pressure drop is out of phase with density wave, positive feedback occurs. This is shown in figure 2.5.

Type III DWOs are caused by the interaction between the inertia and momentum pressure drop terms and the thermo-hydraulic propagation delays. This type of DWOs has received very little attention from researchers (Ruspini, 2013), and are not considered in this thesis.

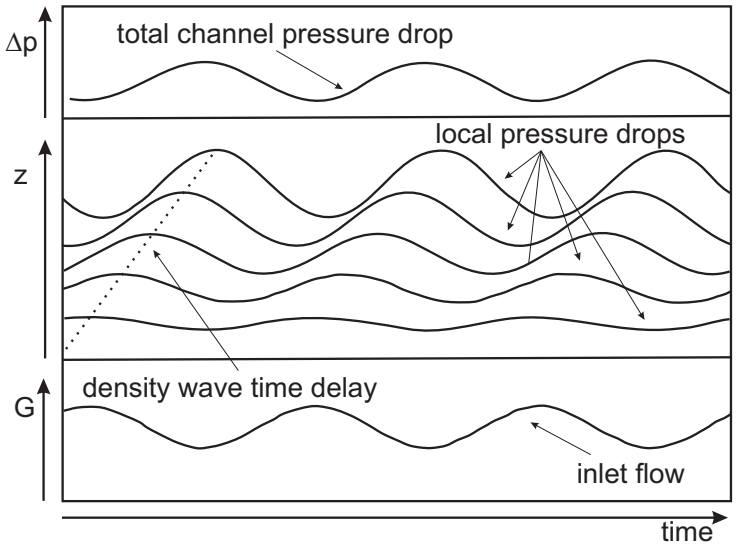


**Figure 2.5:** Density wave oscillation in the core. When the density and pressure drop are 180° out of phase, positive feedback occurs. (Ortega Gómez, 2009)

In a HPLWR water is also the moderator in the reactor, and decrease in density then causes a decrease in moderation, which decreases the core power. This feedback loop is delayed by a time $\tau$, as it takes time for the fission energy released in the fuel rods to be transported through the core wall. It is possible for the core power to get lower when a region of high mass flow passes through and vice versa, thus creating a positive feedback loop, making the system unstable.

## 2.3 Thermal Inertia in tube walls

Note: In a general case, all variables in the next two sections can vary with x, this dependence on x is therefore not used to preserve readability.

Due to the finite dimensions and thermal-physical properties, a tube can absorb and release heat. In a SCWR many flow fluctuations in the tubes are present. One can intuitively feel that if there is a temperature difference between the fluid and tube wall, the tube will affect the flow. Analytical studies by Yuan, Tan, Wen, and Zhuang (2016) have shown that in a pulsating laminar flow, the heat capacity of the tube wall will cause decrease in temperature fluctuations in the flow.

To quantify the effect of thermal inertia we start by looking at an energy balance over the tube wall. This will give us an expression for the heat transferred from and to the wall.

$$\rho c_p V \frac{dT_{wall}}{dt} = P - \alpha_{in}(T_{wall} - T_{fluid})p_{in}dx - \alpha_{out}(T_{wall} - T_{amb})p_{out}dx \tag{2.1}$$

Here $\rho$ and $c_p$ are the density and the specific heat of the wall. $V$ is the volume of the wall over a length element $dx$ and $P$ the power produced in this wall volume element. $T_{wall}$, $T_{fluid}$ and $T_{amb}$ are respectively the temperatures of the wall element, the fluid and the ambient air. $p_{in}$ and $p_{out}$ are the inner and outer perimeter of the tube. $\alpha_{in}$ and $\alpha_{out}$ are respectively the heat transfer coefficient between the tube and the fluid and between the tube and the environment

Equation 2.1 can be understood as follows: The change in thermal energy in the wall with respect to time equals the energy production in tube minus the energy flowing into the fluid minus the energy flowing into the ambient air. It is however important to note that equation 2.1 neglects friction heat and axial heat conduction in the tube. Furthermore it is assumed that there are no differences in wall temperature in the radial and in all azimuthal directions.

We can also find expressions for the linear heating rate: the amount of energy that is transferred into or out of the wall per unit length per unit time.

$$Q'_{in} = \alpha_{in}(T_{wall} - T_{fluid})p_{in} \tag{2.2}$$

$$Q'_{out} = \alpha_{out}(T_{wall} - T_{fluid})p_{out} \tag{2.3}$$

These equations show that energy transfer from the wall is proportional to the temperature difference at a given $\alpha$.

Equation 2.1 shows that there are multiple ways to vary the thermal inertia.

The amount of thermal inertia in the tube wall depends on the heat capacity: the amount of energy needed to change the wall temperature by one degree. It is expressed by:

$$C = \rho c_p V = \rho c_p \frac{\pi(D_{out}^2 - D_{in}^2)L}{4} \tag{2.4}$$

where $C$ is the heat capacity of the tube and $L$ the length of the tube.

Thus to change the amount of thermal inertia, one can change the density, the specific heat or thickness of the wall. To decrease the thermal inertia one of these parameters has to be decreased. Equation 2.1 then says that the wall will then more rapidly follow the temperature of the fluid, which means the temperature difference between the fluid and the wall will get more constant, thus the effect of thermal inertia is decreased.

In the extreme case where one of these parameters is zero, the wall temperature will always follow the fluid temperature instantly, and the difference between the wall and fluid temperature is always constant. This means that there is a constant heat flux and thus no thermal inertia. If there is no power generated in the tube, the temperature difference between the wall and the fluid is zero, and thus there will be no heat flux.

In the other case where the thermal inertia is increased, by increasing one of the aforementioned parameters, the wall temperature will take a longer time to follow the fluid temperature and the temperature difference between the wall and the fluid will fluctuate more, which will increase the effect of thermal inertia.

In the extreme case where one parameter is infinitely large, the wall will always remain a constant temperature. This means the difference in temperature between the wall and the fluid will always fluctuate. If a flow with temperature fluctuations flows in a tube where $T_{wall}$ remains a constant value, the heat flux is expected to remain large and the amplitude of temperature fluctuation are expected to decrease. This reasoning agrees with analytical findings by Yuan et al. (2016).

The heat transfer coefficients $\alpha_{in}$ and $\alpha_{out}$ are found as follows.

$$\alpha_{in} = Nu_{in} \frac{\lambda_{fluid}}{l} \tag{2.5}$$

$$\alpha_{out} = Nu_{out} \frac{\lambda_{air}}{l} \tag{2.6}$$

In equation 2.5 and 2.6 $\lambda$ is the thermal conductivity. Nu is the nusselt correlation, which is depend on the geometry, flow parameters and thermal-physical properties of the media. $l$ is the characteristic length. It is of utmost importance to select the correct characteristic length for the problem.

## 2.4 Natural convection from vertical cylinders

In non-insulated tubes, there is a heat flux to the environment. The heat transfer coefficient $\alpha_{out}$ is proportional on the Nusselt number, as shown in equation 2.6. For free convection from horizontal cylinders, the Nusselt correlations can be found in many textbooks on heat transfer, such as Holman (2010).

For vertical cylinders many of these textbooks only give the criterion for which a vertical cylinder can be approximated as vertical plate.

$$\frac{D}{L} = \frac{35}{{Gr_L}^{0.25}} \tag{2.7}$$

where $D$ is the diameter of the cylinder and $L$ the height-based length of the cylinder. For cylinders that adhere to this criterion, the error is within 5% of the flat-plat solution. (Boetcher, 2014).

$Gr_L$ in equation 2.7 is the height based Grashof number. The Grashof number can be physically interpreted as the ratio of the buoyancy forces to the viscous forces in the free-convection flow system (Holman, 2010). It is defined:

$$Gr_L = \frac{g\beta(T_{wall} - T_{amb})L^3}{\nu^2} \tag{2.8}$$

Here g is the gravitational acceleration, $\beta$ the thermal expansion coefficient and $\nu$ the kinematic viscosity.

Note: for vertical surfaces, the Grashof Number and Nusselt Number are always formed using a height-based length of the surface as the characteristic length (Holman, 2010). This gives us the following expression for the heat transfer coefficient $\alpha_{out}$:

$$\alpha_{out} = Nu_{out}\frac{\lambda_{air}}{L} \tag{2.9}$$

where L is the height of the cylinder.

When the criterion in equation 2.7 does not hold, a different Nusselt correlation be for vertical cylinders must be used. One can derive an expression for a Nusselt correlation using an integral method, as done by Ede (1967). This paper by Ede (1967) contained two Nusselt correlations: one for the local Nusselt number and one for a length averaged Nusselt number. The results are shown in equations 2.10 and 2.11.

$$Nu_{out} = \left(\frac{7Gr_x Pr_{out}^2}{5(20+21Pr_{out})}\right)^{\frac{1}{4}} + \frac{4(272+315Pr_{out})x}{35(64+63Pr_{out})D_{out}} \tag{2.10}$$

$$Nu_{out} = \frac{4}{3}\left(\frac{7Gr_L Pr_{out}^2}{5(20+21Pr_{out})}\right)^{\frac{1}{4}} + \frac{4(272+315Pr_{out})L}{35(64+63Pr_{out})D_{out}} \tag{2.11}$$

In equation 2.10 $x$ is the height coordinate of the cylinder, and $Gr_x$ is the local Grashof number at coordinate $x$. It is defined as $Gr_x = \frac{g\beta(T_{wall}-T_{amb})x^3}{\nu^2}$. $Pr$ is the Prandtl number, which is defined as the the ratio of momentum diffusivity to thermal diffusivity (Coulson, Richardson, Backhurst, & Harker, 1999). In equation form: $Pr = \frac{\nu}{a}$ where a is the thermal diffusivity. The Prandtl number is independent of a length scale, and solely dependent on the fluid state and properties. The characteristic lengths for these correlations are respectively $L$ and $x$.

Using an ideal gas approximation, $\beta$ can be expressed as $\beta \approx \frac{1}{T_{avg}}$. $T_{avg}$ here is the average temperature between the wall and the ambient air.

# Chapter 3

# DeLight experiment

The DeLight facility was a scaled version of a natural circulation driven HPLWR that used Freon R23 scaling fluid instead of water, the scaling rules were derived by Rohde, Marcel, T'Joen, Class, and van der Hagen, 2011. Freon R23 has its critical point at 4.83 MPa and 26.14°C. This allowed facility to operate at a lower pressure of 5.7 MPa compared to 25 MPa and on a lower temperature range of -30 – 100°C, instead of the SCWR operating temperature range of 280 – 500°C. This scaling allowed for a reduction in structural requirements for the facility. Furthermore the facility had an artificial neutronic feedback system dependent on the density of the fluid with a time constant $\tau$ of 6 seconds (T'Joen & Rohde, 2012). Table 3.1 gives an overview of the critical and pseudocritial properties of Freon R-23 and water in respectively the DeLight facility and the HPLWR.

**Table 3.1:** Comparison of the critical and pseudocritical properties of Freon R23 and water in the DeLight and HPLWR.

| | **Freon R-23** | **Water** |
|---|---|---|
| Critical pressure (MPa) | 4.83 | 22.06 |
| Critical temperature (°C) | 26.14 | 373.95 |
| operating pressure (MPa) | 5.70 | 25.00 |
| Operating temperature range (°C) | -30 – 100 | 280 – 500 |
| $h_{pc}$ ($Jkg^{-1}K^{-1}$) | 288.33 | 2152.90 |
| $T_{pc}$ (°C) | 33.22 | 273.95 |

## 3.1 Geometry and components

The DeLight setup was a single channel loop consisting of a three-pass core made out of 6 mm inner diameter stainless steel pipe with a thickness of 0.5 mm. The three heated core-sections are called the evaporator, superheater I and superheater II. Each core-section was 0.8m long. The core was heated using by running a current high through the tube wall(up to 600 A per core-section). The power distribution in the core was the same as in a HPLWR, with 53% in the evaporator,30 in superheater I and 17% in superheater II. Inbetween the three heated core section, are 2 unheated intermediate tube sections. These sections have the same dimensions are the core sections, but are not heated.

After the core-section is an 8.2 m long riser. Outside of the core-sections the tube has an inner diameter of 10 mm, 1 mm thickness and is insulated using 25 mm Armacell to prevent heat loss to the environment. This is followed by two heat exchangers, that simulate the turbine and condenser in a HPLWR. The first heat exchanger brings down the temperature to 17 °C and the second heat exchanger reduces the desired core inlet temperature. At the end of the heat exchangers, the downcomer begins. The downcomer has a preheater that was sometimes used to more accurately set the desired core inlet temperature. At the top of the loop is a buffer vessel to ensure the pressure remains constant throughout the loop. Throughout the loop there are various sensors to measure the temperature, flow and density. A schematic overview of the entire facility is given in figure 3.1. A detailed technical drawing can be found in Appendix A.

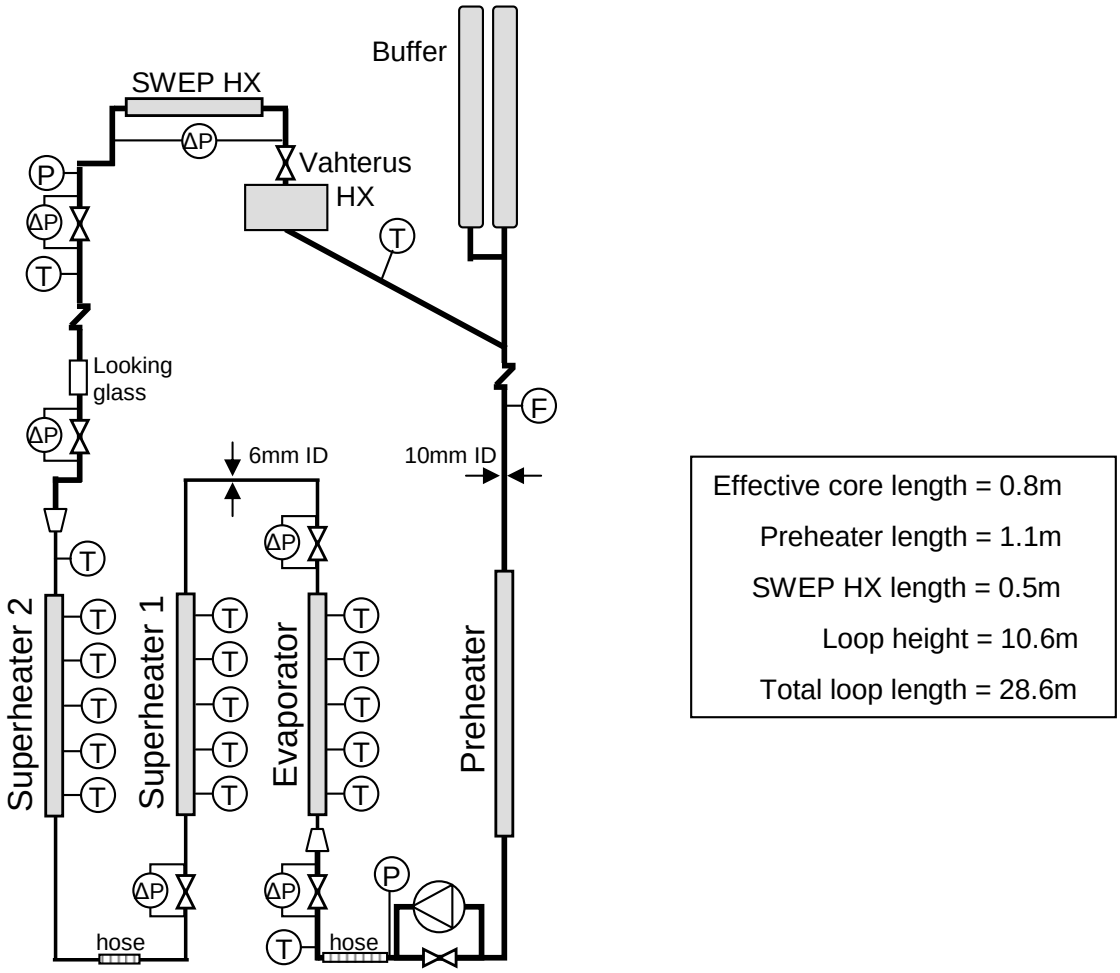


**Figure 3.1:** Schematic overview of the DeLight Facility. The riser and downcomer are shortened to save space. The three core sections are the evaporator, superheater I and superheater II. Inbetween the evaporator and superheater I, and superheater I and superheater II, is an intermediate tube. A detailed technical drawing can be found in Appendix A.

## 3.2 Measurements

A measurement in the DeLight facility is started using an electrical pump at the bottom of the loop. The core power is then gradually increased and the pump is turned off. After some time the system will reach a steady state flow. To analyze the stability of the reactor, the neutronic feedback system is turned on and the core power is increased by 250-500 W for 5 seconds. This perturbation causes a oscillation in the flow. By looking if this oscillation decays or grows over time, the system is respectively stable or unstable.

To quantify the amount decay/growth, a decay ratio is defined. By fitting the function $y = (1 - c_1 - a_1)e^{b_1 t} + c_1 + a_2 e^{b_2 t}\cos(\omega t)$ to the first two periods of the auto correlation function of the temperature oscillation (T'Joen & Rohde, 2012), a decay ratio is then defined as:

$$DR = e^{\frac{2\pi b_2}{|\omega|}} \tag{3.1}$$

# Chapter 4

# Numerical code

To study the effect of wall thermal inertia in the riser on the flow stability in the DeLight setup, a numerical code has been used. A detailed description of the numerical model can be found in Spoelstra (2012). This section 4.1 aims to give a brief overview of the numerical methods used in this code. Section 4.2 describes the adjustments in the implementation of the wall thermal inertia in the riser. Furthermore corrections in the model for free convection around the heated core sections are discussed in section 4.3

## 4.1 DeLight model

The numerical code for the DeLight model uses a 1D finite volume method with first order upwind scheme. In time multiple descretization schemes are implemented:

1. A fully implicit backward Euler scheme
2. A fully explicit forward Euler scheme
3. A semi-implicit combination of forward and backward Euler scheme

The fully implicit scheme is unconditionally stable, even at large time steps, but computationally demanding and less accurate than the other methods. The fully explicit scheme is accurate and computationally cheap, however requires small time steps in order to remain stable.

The semi-implicit scheme is a combination of an implicit and explicit scheme. In this scheme the parameter $\theta$ is introduced as balancing parameter between the two schemes. $\theta$ has a value between 0 and 1, when $\theta = 1$ a fully explicit scheme is used and if $\theta = 0$ a fully implicit scheme is used. For values in-between 0 and 1 a proportional ratio of both schemes is used. In this thesis the value $\theta = 0.6$ is used as semi-implicit model.

The goal of using a semi-implicit scheme is to use a significantly larger time step than a fully explicit scheme, while keeping the numerical model stable and without sacrificing much accuracy (Fulton, 2004).

In order to prevent odd-even decoupling of the pressure field, a staggered grid was implemented in the code (Patankar, 1980). The momentum balance is solved in control volumes around points with index i, while the enthalpy balance and continuity equation are solved over control volumes around index j. This is shown in figure 4.1.

A complete flowchart of the numerical DeLight model is fond in appendix B.

## 4.2 Implementation of thermal inertia in the tube walls

Schenderling (2013) discretized the energy balance equation 2.1 and implemented this in the DeLight model to study the effect of thermal inertia in the heated core section on the stability of the system. A full explanation and derivation of the descretization can be found in (Schenderling, 2013).

This same implementation has been extended to include the riser and the non-heated section of the core. The difference is that the power production in the core in these section is zero, and that the tubing is insulated, so there is no loss due to free convection to the ambient air.

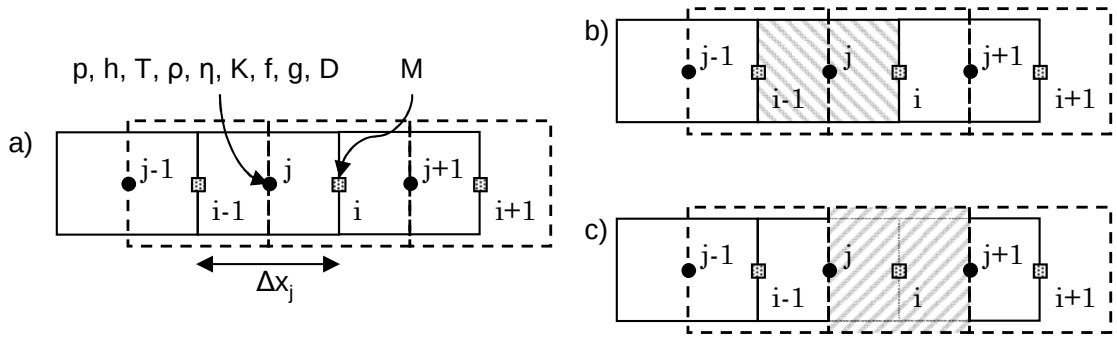


**Figure 4.1:** a) Schematic overview of control volumes for a staggered grid. b) The enthalpy balance and continuity equation are solved over the shaded control volumes around indices j. c) the momentum balance is solved over the shaded control volumes around index i. (Spoelstra, 2012)

## 4.3 Natural convection from the core wall the the environment

A model for natural convection was implemented by Schenderling (2013). He implemented a Nusselt and Grashof correlation for the average free convection from the core, however used incorrect characteristic lengths for both of the correlation, namely he used the diameter as characteristic length instead of the Height. This mistake has been corrected. Furthermore the effect of correlations for local Gr and Nu at are studied, where

$$Gr_x = \frac{g\beta(T_{wall} - T_{ambient})x^3}{\nu^2} \qquad \text{and} \qquad Nu_{out} = \left(\frac{7Gr_x Pr_{out}^2}{5(20 + 21Pr_{out})}\right)^{\frac{1}{4}} + \frac{4(272 + 315Pr_{out})x}{35(64 + 63Pr_{out})D_{out}}$$

The results of these changes are shown in chapter 6.3.

# Chapter 5

# Experimental procedure

In order to analyze the stability of the system, first a steady state solution has to be found. This is described in section 5.1. The methodology of describing the stability of the system is described in section 5.2.

## 5.1 Acquiring a steady state solution

To analyze the stability of the DeLight model, a steady state solution is needed. This solution is obtained by solving the time-dependent transport equations, while increasing the core power from zero to its specified level over a certain time, $t_{warmup}$. After this period, the core power remains constant at its specified power and the model is given some time to converge to the steady state solution. Finally, at a time $t_{steady}$, the system is assumed to be in a steady state.

The increase in core power follows an S-shaped function(Spoelstra, 2012), which is given by the following:

$$P_{core}(t) = \begin{cases} P_{sp}\left(1 - e^{\left(\frac{-2.1t}{t_{warmup}}\right)^3}\right) & \text{for } 0 \leq t < t_{warmup} \\ P_{sp} & \text{for } t \geq t_{warmup} \end{cases} \tag{5.1}$$

Here $P_{core}$ is the core power at time $t$, $P_{sp}$ the specified core power and $t_{warmup}$ the warm up time.

For the steady state simulations fully implicit model is used, as it allows for much larger time steps $dt$ to be used. This keep the computational cost down. To ensure a positive mass flow, the system is started with a small finite flow in the positive direction.

In this thesis the following values are used to acquire a steady state solution:

$$t_{warmup} = 2000 \text{ s}, \; t_{steady} = 2500 \text{ s and } dt = 1 \text{ s}.$$

## 5.2 Stability analysis

To analyze the system's stability, a new simulation is started with the steady state solution as initial condition. This new simulation utilizes the semi-implicit scheme with $\theta = 0.6$, as a value closer to 0.5 led to model instabilities(Spoelstra, 2012). The semi-implicit scheme has a higher computational cost and requires much smaller time steps in order to be remain stable, compared to the implicit scheme, but has a reduced amount of numerical diffusion and is more accurate.

The stability of the DeLight Model is done is the same manner as in the DeLight experimental measurements. An oscillation in the flow can be induced by applying a perturbation to a system variable. According to Spoelstra (2012) the change from implicit to semi-implicit model caused a large enough perturbation to analyze the stability. In many cases this seems to be true, however there are quite a few cases where the perturbation caused by the change of discretization scheme is too small, and the effect of numerical diffusion relatively large. To reduce the effect numerical diffusion, the perturbation was started by increasing the core power by 5% for 1 second. The resulting perturbation is larger and, consequently, the effect of numerical diffusion relatively smaller. This way of starting the perturbation is similar to the way the the experimental DeLight measurements were performed, where the core power was increased by 250 - 500 W for 5 seconds.

To determine the stability of the system, the decay or growth of the oscillation is observed. To quantify the stability the decay ratio (DR) is used. Again the function $y = (1 - c_1 - a_1)e^{b_1 t} + c_1 + a_2 e^{b_2 t}\cos(\omega t)$ is fit against the first to periods of the oscillation in the temperature signal. The decay ratio is also the same as in equation 3.1: $DR = \exp\left(\frac{2\pi b_2}{|\omega|}\right)$

A $DR > 1$ indicates a point which is unstable, while $DR < 1$ indicates a stable point. When $DR = 1$ a perturbation on the system will neither grow nor decay. These stable and unstable points are mapped onto a dimensionless plane spanned by two dimensionless numbers: The pseudo phase change number $N_{PCH}$ and the subcooling number $N_{SUB}$. These dimensionless numbers are defined as follows(T'Joen & Rohde, 2012):

$$N_{SUB} = \frac{h_{pc} - h_{in}}{h_{pc}} \tag{5.2}$$

$$N_{PCH} = \frac{P_{core}}{\dot{m} h_{pc}} \tag{5.3}$$

Where $h_{in}$ is the enthalpy at the core inlet, $h_{pc}$ the enthalpy at the pseudocritical temperature, $P_{core}$ the core power and $\dot{m}$ the mass flow rate. For Freon R23 at 5.7 MPa $h_{pc} = 288.22 Jkg^{-1}K^{-1}$

$N_{SUB}$ is a dimensionless measure for the enthalpy at the core inlet. A high inlet enthalpy gives a low $N_{SUB}$. By extend this can also be interpreted as a high inlet temperature, $T_{in}$, which gives a low $N_{SUB}$.

$N_{PCH}$ is dependent on the core power and the mass flow rate. In a natural circulation driven system $\dot{m}$ is no longer a independent parameter, but it is now a function of $P_{core}$. Physically $N_{PCH}$ can be interpreted as the enthalpy gain of the fluid through out the core.

All working points of the DeLight are represented by a combination of $P_{core}$, $T_{in}$ and $\dot{m}$, which can be expressed as set of $N_{PCH}$ and $N_{SUB}$.

## 5.3 Validation of the thermal inertia model

In order to validate if the thermal inertia model works is correct, the model is compared to the results of Van Iersel (2016). Van Iersel's DeLight model only had thermal inertia in the heated core sections. As shown in chapter the amount of thermal inertia in the tube wall can be varied by changing the heat capacity, which is expressed as in equation 2.4: $C = \rho c_p \frac{\pi(D_{out}^2 - D_{in}^2)L}{4}$.

To approximate the results obtained Van Iersel, 2016, the thermal inertia outside of the heated core sections has to be zero, ie. the riser and intermediate tubes between the three core sections. These sections can be found in 3.1. This can be achieved in a few ways: the density, the specific or the thickness of the wall can be set to approach zero outside the heated core sections. Here it is chosen to change the thickness.

The wall thickness cannot be set to exactly zero as the numerical model will then divide by zero. Therefore the thickness has been set to $10^{-15}$m. This value is deemed small enough to approximate an infinitely thin wall, as it is thinner than an atom.

# Chapter 6

# Results and discussion

This chapter shows the results of the numerical simulations and discusses these. Section 6.1 shows the validity of the implemented model by comparing it to simulations done by Van Iersel (2016). Section 6.2 shows the effect of effect of thermal inertia on the stability of DeLight. And finally section 6.3 show the effect of the correction made on the model for natural convection from the core.

**Table 6.1:** Overview of all the simulations settings used to obtain the results in this chapter. $\delta$ denotes the wall thickness.

| **model description** | $\delta_{wall}$ | $\delta_{intermediatetube}$ | **natural convection model** |
|---|---|---|---|
| Thin wall approximation | $10^{-15}$ m | $10^{-15}$ m | Incorrect natural convection |
| DeLight geometry | $10^{-3}$ m | $0.5 \cdot 10^{-3}$ m | Incorrect natural convection |
| Approximation with thermal inertia in the intermediate tubes | $10^{-15}$ m | $0.5 \cdot 10^{-3}$ m | Incorrect natural convection |
| Riser wall thickness variation | $10^{-15}$ – $10^{2}$ m | $0.5 \cdot 10^{-3}$ m | Incorrect natural convection model |
| Length-averaged natural convection | $10^{-3}$ m | $0.5 \cdot 10^{-3}$ m | Length-averaged natural convection model |
| Local natural convection | $10^{-3}$ m | $0.5 \cdot 10^{-3}$ m | Local natural convection model |

## 6.1 Validation of the thermal inertia model

To prove the validity of the thermal inertia model, the model is used to approximate the results obtained by Van Iersel (2016). Setting the wall thickness in the riser and the intermediate tubes, between the core sections. $10^{-15}$ m gives the following result:

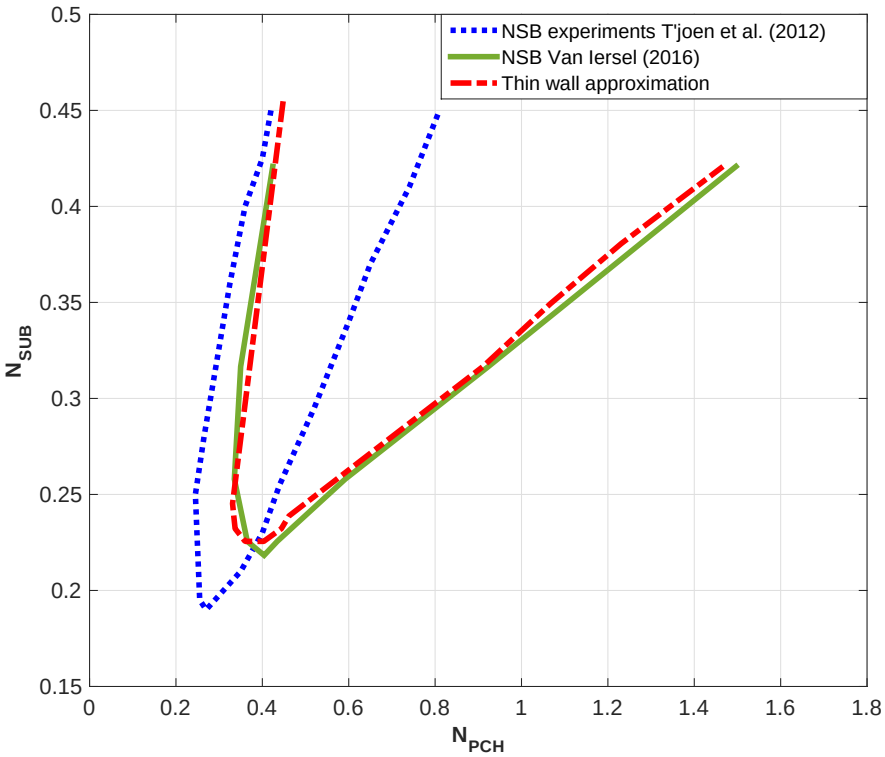


**Figure 6.1:** Approximation of the NSB by Van Iersel, by setting the wall thickness of the riser and intermediate tubes to $10^{-15}$ m

The thermal inertia model seems to properly approximate the results obtained by Van Iersel (2016). The approximation seems to be slightly more stable. This is likely because of the the interpolation between the stable and unstable points. Choosing slightly different points for the simulation, can change the position of the NSB. Additionally the thermal inertia is not truly zero, so a slightly more stable system is expected. Lastly the difference between the two is small, and the approximation could be within the uncertainty in the results by Van Iersel (2016). Based on this result the model is assumed to correctly describe the effects of thermal inertia.

## 6.2 Effect of thermal inertia in the riser on the stability of the DeLight model

First, the actual geometry of the DeLight facility was used to examine the stability. This means the riser wall thickness is 1 mm and the thickness of both the heated and unheated sections of the core wall are set to 0.5 mm. The result is shown in figure 6.2.

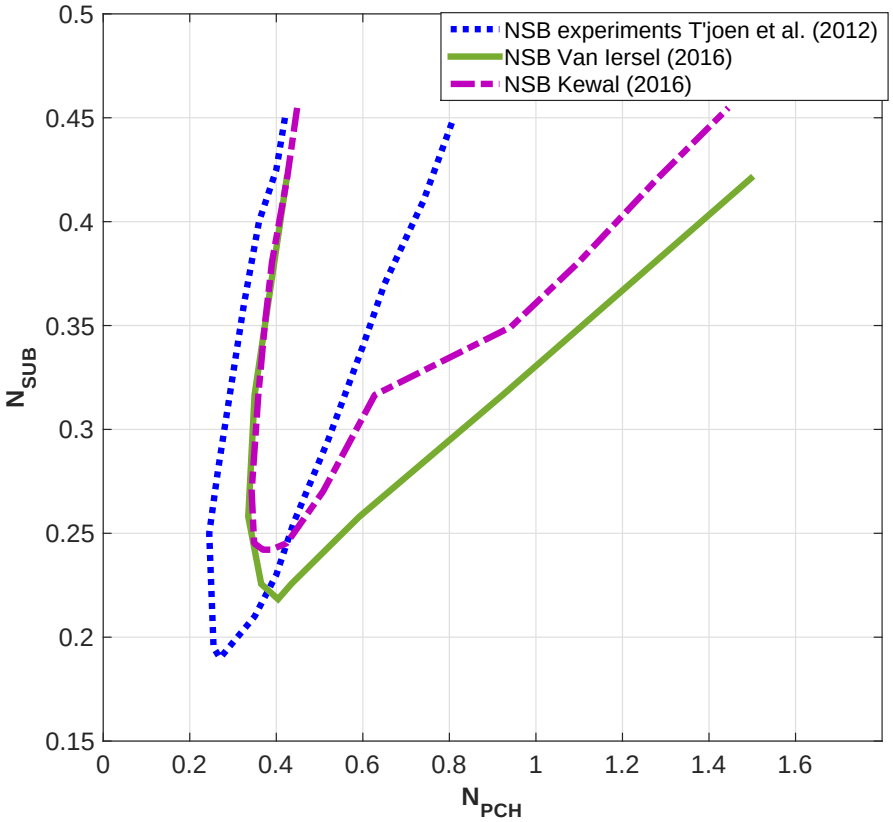


**Figure 6.2:** NSB found using the thermal inertia models and the geometry of the DeLigtht facility with 1 mm thick riser wall and 0.5 mm core wall.

It can be see that the system is significantly more stable than the NSB by Van Iersel (2016) at high $N_{PCH}$. At low $N_{PCH}$, where type I DWOs are more prevalent, the stability does not seem to change. This means the change in stability is mainly due to frictional effects. Since the riser wall now has a heat capacity and, consequently, temperature, there is a flux between the wall and the Freon R23, which dampens out temperature oscillations as explained in chapter 2.3. Additionally Van Iersel (2016) showed that that the friction factor decreased when the fluid and wall were no longer isothermal. This decrease in the friction factor causes a decrease in pressure drops due to friction, which, subsequently, reduces the effect of type II DWOs.

The above analysis includes the thermal inertia in both the heated core sections and the intermediate tubes. The effect of only the intermediate tube sections is analyzed by setting the riser wall thickness to zero, while keeping the thickness of the intermediate tube sections unchanged. The result is shown in figure 6.3.

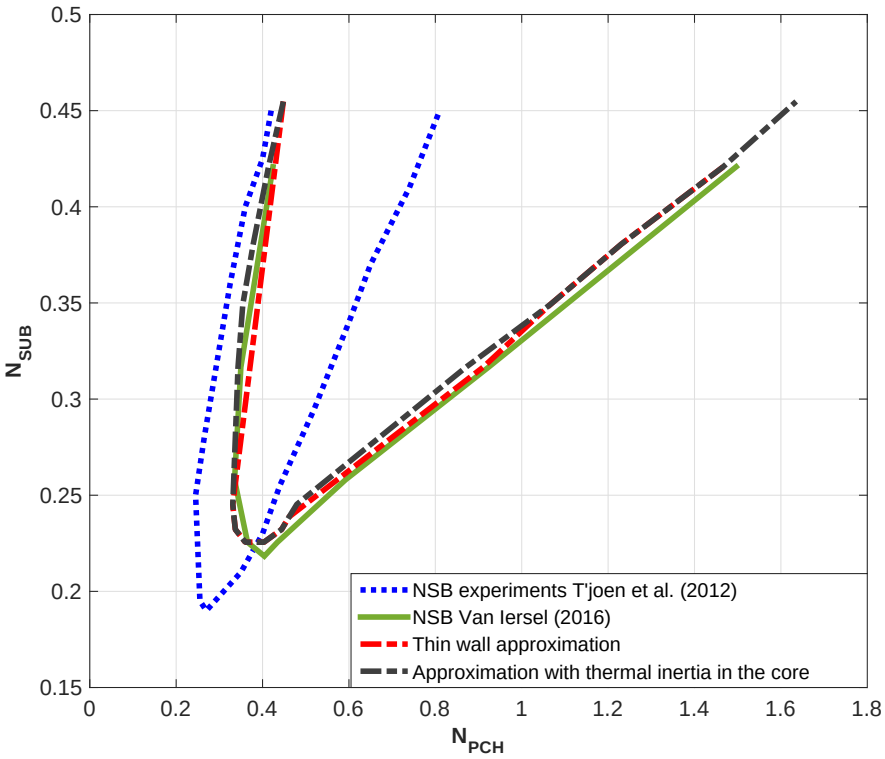


**Figure 6.3:** Approximation of the NSB by Van Iersel, with thermal inertia in the intermediate tube sections.

It can be seen that the intermediate tube sections have an effect, however it is extremely small. Therefore it can now be safely concluded that the change in stability in figure 6.2 was caused by the thermal inertia in the riser.

Next the thickness of the wall was varied, to analyze the effect of different amounts of thermal inertia in the riser. The core sections were unchanged at its actual value. It is expected that a thicker wall will have stabilizing effect on the system, since there is more thermal inertia. The thermal inertia should reduce the amplitude of fluctuations in temperature difference between the wall and fluid. Figure 6.4 shows the neutral stability line for different riser wall thicknesses. Figure 6.5 zooms in on the minimum of the NSB.

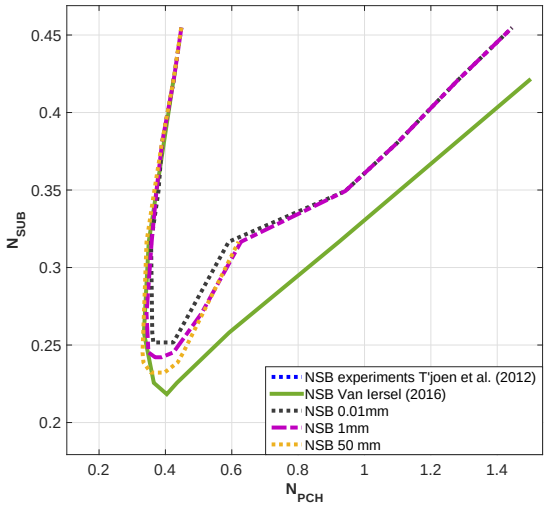


**Figure 6.4:** NSB for Different wall thicknesses. It can be seen that at the minimum of the NSB the system becomes more unstable for a thicker wall.

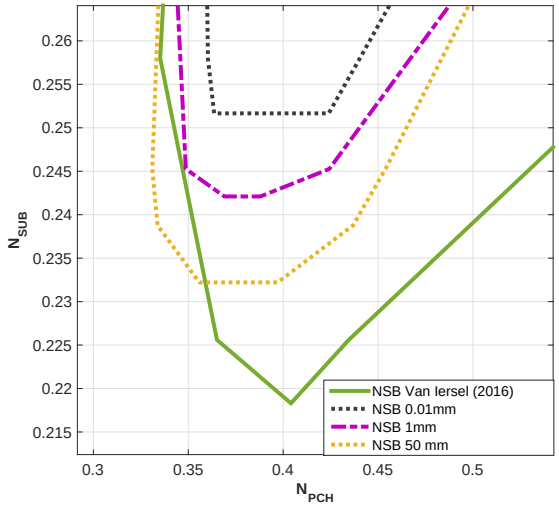


**Figure 6.5:** Zoom in on the minima of the NSBs of different thicknesses in figure 6.4.

It can be seen that the system becomes more unstable with with thicker walls. For high $N_{PCH}$ the the stability does not seem to be affected by the riser thickness. This means that the amount of heat flux exchanged in the riser is small.

To see a trend in the how the stability depends on thickness, the stability is analyzed in the same points for multiple wall thicknesses, by looking at the decay ratio in a single point. The point chosen for this is the minimum of the NSB for the 1 mm thick wall, where ($N_{SUB}$,$N_{PCH}$) = (0.39706, 0.24526). This plot shown in figure 6.6.

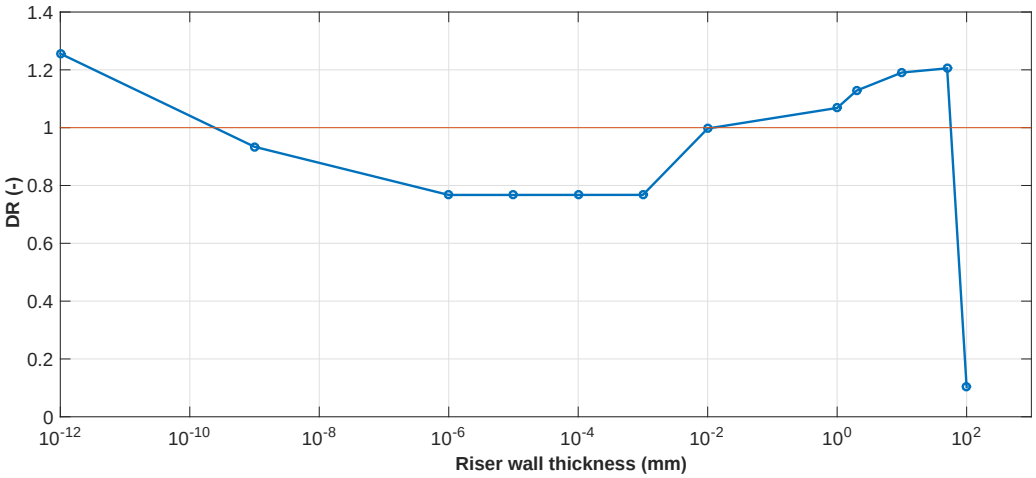


**Figure 6.6:** Plot of the decay ratio vs riser wall thickness. It can be seen that the DR grows to a local maximum at 50 mm. At 100mm the system becomes very stable.

The decay ratio seems to have a local maximum at 50 mm, where its the most unstable. Additionally, at $10^{-4}$ mm, there is a local minimum. At 100 mm, the working point becomes very stable. Wall thicknesses larger than 100 mm, gave numerical instabilities and could not be evaluated. No clear explanation for this minimum and maximum was found.

## 6.3 Corrections on the heat transfer correlations for natural convection around the core

Schenderling (2013) had used an incorrect characteristic length for his models in free convection. Two models had been proposed in the chapter 4.3, one for an average Nusselt number for each core section, and one the the local Nusselt number in every control volume. Both models were run in combination with the thermal inertia model from the previous section for a 1 mm thick riser wall and 0.5mm thick core. The results of both these models is shown in figure 6.7.

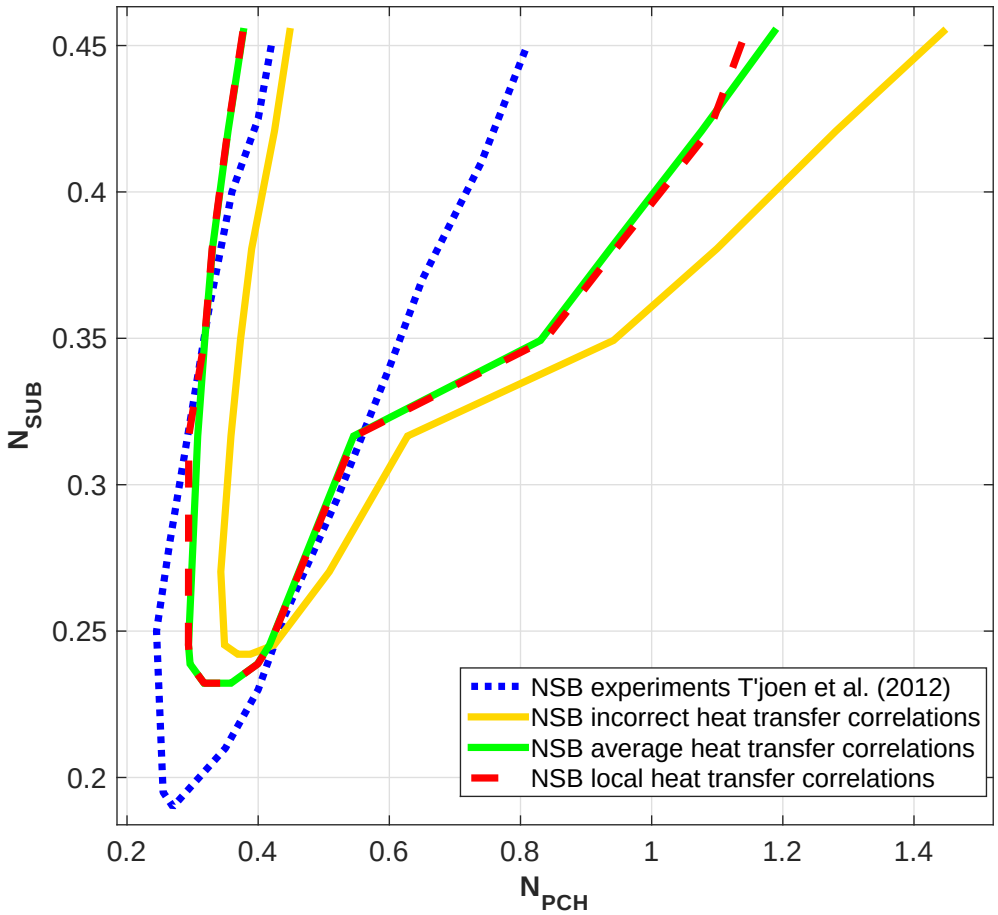


**Figure 6.7:** Plot of the NSB using the old incorrect model by Schenderling (2013) for free convection around the heated core section, the model for the average free convection and the model for the local free convection around the core.

It can be seen that a correct model for natural convection has a significant effect on the stability. Both the local and average model are virtually identical, the differences are small and likely within the uncertainty of each other.

The resulting NSB with a correct model for the natural convection closely resembles the experimental NSB for low and medium powers. For higher $N_{PCH}$ the numerical model shows a less stable results than the experimental results. This could be due to several assumptions made in the model. For example axial and radial heat transfer in the wall and bulk are neglected. The heat exchangers and preheater are not properly modeled in the current DeLight model. The heat exchanger is modeled as an enthalpy forcing function that bring the temperature down to the inlet temperature. The preheater is not modeled with thermal inertia.

## 6.4 Overview of neutral stability boundaries

This section serves as a overview of stability boundaries found by T'Joen and Rohde (2012), Spoelstra (2012), Schenderling (2013), Van Iersel (2016) and Kewal (2016). To get an overview of how different physical mechanisms affect the NSB, it is useful to plot all NSBs in one plot. This is shown in figure 6.8.

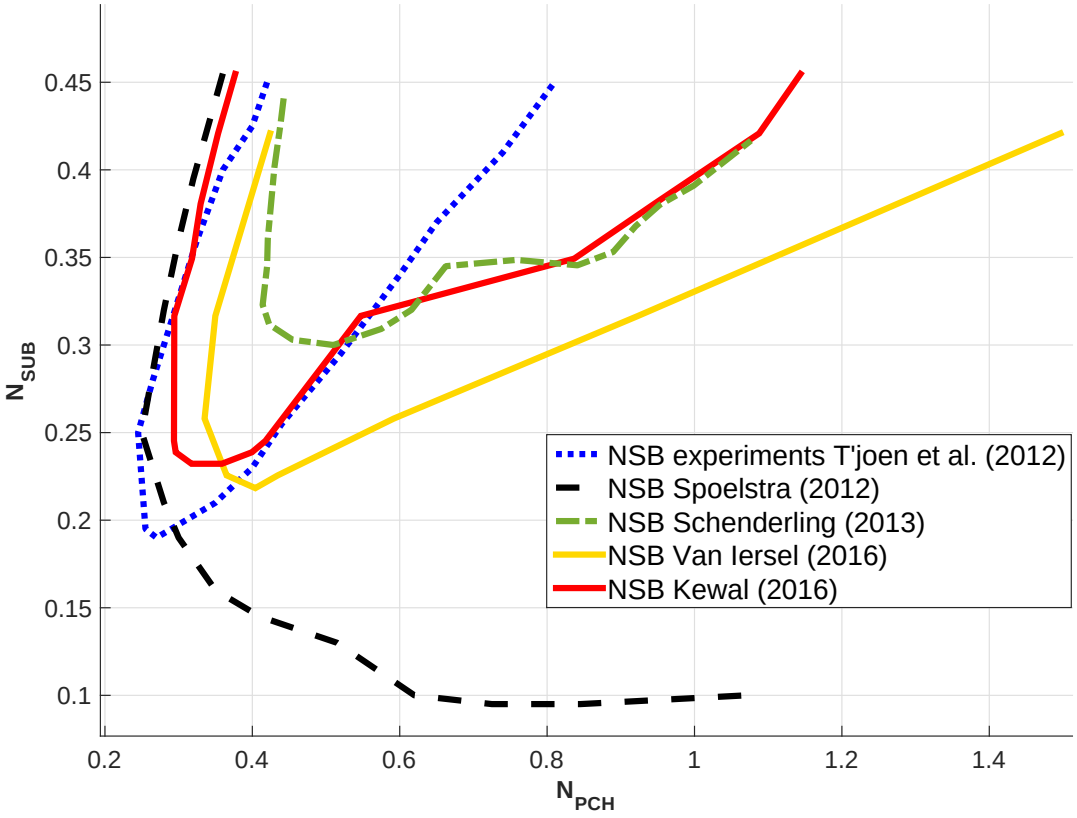


**Figure 6.8:** plot of all NSBs as found by T'Joen and Rohde (2012), Spoelstra (2012), Schenderling (2013), Van Iersel (2016) and Kewal (2016). This plot serves as reference to compare the different NSBs.

T'Joen and Rohde (2012) conducted the experimental study on the DeLight facility. Spoelstra (2012) used a model without thermal inertia, with a constant heat flux from the heated core sections and with a constant loss. Schenderling (2013) implemented thermal inertia in the core, however he implemented and in correct natural convection model. Van Iersel (2016) added friction and heat transfer correlations for supercritical flow to the model. Kewal (2016) added thermal inertia in the riser and corrected the natural convection model from the core to the environment.

By looking at the the position of the different NSBs, we can see how the stability changes with adjustments in the model. This helps give an understanding of the mechanisms in play in the system.

# Chapter 7

# Conclusions

## 7.1 Conclusions

The aim of this thesis was to study the effect of wall thermal inertia in the riser on the stability of the DeLight model and to see if experimental results could be reproduced using the numerical model. In order to do so the thermal inertia model implemented by Schenderling (2013) was extended to the riser.

The model was validated by approximating results found by Van Iersel (2016), where there was only thermal inertia in the heated core sections. This was done by numerically changing the wall thickness outside of the heated core sections to $10^{-15}$. The new model properly approximated the results by Van Iersel (2016), thus it was concluded that the model was correct.

Modeling the actual DeLight geometry using the new model, resulted in a more stable system than predicted by Van Iersel (2016). The thermal inertia greatly stabilized the system in the region where Type II DWOs are prevalent. Type I DWOs seemed to not be affected much.

Next the amount of thermal inertia was varied by varying the wall thickness. In contrast to what was expected, more thermal inertia made the system less stable. By looking at the Decay ratio against the thickness in one operational point, it could be seen that a wall already made the system more stable. This means that only a small of thermal inertia is enough to stabilize the system. A plot of wall thickness vs decay ratio showed a stable local minimum for $10^{-4}$ mm and an unstable local maximum for 50 mm. No clear explanation for this minimum and maximum was found.

Finally a correction on the natural convection from the heated core sections was implemented. Schenderling (2013) had used an incorrect characteristic length in his heat transfer model. Two different models have been used compared: a model using the average Nusselt number in each core section, and a model using the local Nusselt number in each control volume. Both resulted in a nearly identical NSB. The discrepancies are likely to be within the uncertainty of each other.

## 7.2 Outlook

There are still discrepancies between the experimentally measured NSB by T'Joen and Rohde (2012) and the results obtained in this thesis. Several phenomena have still been neglected, such as friction heat, axial and radial heat transfer in the wall and bulk. The heat exchangers and downcomer have also not been properly modeled, for example the heat exchanger is modeled in a non physical way as an enthalpy forcing function.

Numerical diffusion also plays a role, although this is not expected to have a very large effect. The effects of numerical diffusion have already been reduced in the methodology of this thesis and the system is more unstable than the experimental results, and numerical diffusion has a stabilizing effect.

Further research is also needed to explain the minimum and maximum found in fig 6.6, where the system becomes more stable as the riser wall thickness is increased up until 0.1 mm and then destabilizes when the thickness is further increased to 50 mm. At 100 mm the system was found to be very stable.

# Bibliography


Boetcher, S. K. (2014). *Natural convection from circular cylinders*. Springer.

Boure, J., Bergles, A., & Tong, L. S. (1973). Review of two-phase flow instability. *Nuclear Engineering and Design*, *25*(2), 165–192.

Bouré, J., Bergles, A., & Tong, L. S. (1973). Review of two-phase flow instability. *Nuclear Engineering and Design*, *25*(2), 165–192.

Collins, D. & Gacesa, M. (1969). Hydrodynamic instability in a full-scale simulated reactor channel. In *Proceedings of the institution of mechanical engineers, conference proceedings* (Vol. 184, *3*, pp. 115–126). SAGE Publications.

Coulson, J., Richardson, J., Backhurst, J., & Harker, J. (1999). *Coulson and richardson's chemical engineering volume 1 - fluid flow, heat transfer and mass transfer* (6th Edition). Elsevier.

Ede, A. (1967). Advances in free convection. *Advances in heat transfer*, *4*, 1–64.

Fang, X., Xu, Y., Su, X., & Shi, R. (2012). Pressure drop and friction factor correlations of supercritical flow. *Nuclear Engineering and Design*, *242*, 323–330.

Fulton, S. R. (2004). *Semi-implicit time differencing*. Citeseer.

Holman, J. P. (2010). *Heat transfer, tenth edition (mcgraw-hill series in mechanical engineering)*. The McGraw-Hill Companies, Inc.

Kam, F. (2011). *Development of a one-dimensional computer model for the stability analysis of a natural circulation super critical water reactor* (Master's thesis, Delft University of Technology, The Netherlands).

Koopman, H. (2008). *Development of the stealth-code and investigation of the effects of feedwater sparger positioning on the thermal-hydraulic stability of natural circulation boiling water reactors* (Master's thesis, Delft University of Technology, The Netherlands).

Ledinegg, M. (1938). Instability of flow during natural and forced circulation. *Die Warme*, *61*(8), 891–898.

Oka, Y., Koshizuka, S., Ishiwatari, Y., & Yamaji, A. (2010). *Super light water reactors and super fast reactors: supercritical-pressure light water cooled reactors*. Springer Science & Business Media.

Ortega Gómez, T. (2009). Stability analysis of the high performance light water reactor. *Wissenschaftliche Berichte FZKA*, *7432*.

Patankar, S. (1980). *Numerical heat transfer and fluid flow*. CRC press.

Pioro, I. & Mokry, S. (2011). Thermophysical properties at critical and supercritical conditions. *Heat Transfer Theoretical Analysis, Experimental Investigations and Industrial Systems. InTech, Rijeka*.

Rohde, M., Marcel, C., T'Joen, C., Class, A., & van der Hagen, T. (2011). Downscaling a supercritical water loop for experimental studies on system stability. *International Journal of Heat and Mass Transfer*, *54*, 65–74.

Ruspini, L. C. (2013). Experimental and numerical investigation on two-phase flow instabilities.

Schenderling, T. (2013, July). *Numerical analysis of the influence of wall thermal inertia on the stability of natural circulation driven supercritical water reactors* (Bachelor Thesis, Delft University of Technology).

Schulenberg, T., Starflinger, J., & Heinecke, J. (2008). Three pass core design proposal for a high performance light water reactor. *Progress in Nuclear Energy*, *50*(2), 526–531.

Spoelstra, J. (2012). *Numerical stability analysis of natural circulation driven supercritical water reactors* (Master's thesis, Delft University of Technology, The Netherlands).

Squarer, D., Schulenberg, T., Struwe, D., Oka, Y., Bittermann, D., Aksan, N., ... Dumaz, P. (2003). High performance light water reactor. *Nuclear Engineering and Design*, *221*(1), 167–180.

T'Joen, C. & Rohde, M. (2012). Experimental study of the coupled thermo-hydraulic–neutronic stability of a natural circulation hplwr. *Nuclear Engineering and Design*, *242*, 221–232.

Tsiklauri, G., Talbert, R., Schmitt, B., Filippov, G., Bogoyavlensky, R., & Grishanin, E. (2005). Supercritical steam cycle for nuclear power plant. *Nuclear Engineering and Design*, *235*(15), 1651–1664.

Van Iersel, M. (2016, January). *Effect of supercritical friction factor and heat transfer model on the stability of a natural circulation driven super critical water reactor* (Bachelor Thesis, Delft University of Technology).

Yuan, H., Tan, S., Wen, J., & Zhuang, N. (2016). Heat transfer of pulsating laminar flow in pipes with wall thermal inertia. *International Journal of Thermal Sciences*, *99*, 152–160.

# Nomenclature

| Symbol | Dimensions | Description |
|---|---|---|
| Roman Symbols | | |
| C | $J/K$ | Heat capacity |
| $c_p$ | $J/kgK$ | Specific heat |
| D | $m$ | Diameter |
| L | $m$ | Height-based length |
| l | $m$ | Characteristic length |
| $\dot{m}$ | $kg/s$ | Mass-flow |
| P | $W$ | Power |
| p | $m$ | Perimeter |
| $\mathcal{P}$ | $Pa$ | Pressure |
| $Q'$ | $W/m$ | Linear heating rate |
| T | $K$ | Temperature |
| t | $s$ | time |
| V | $m^3$ | Volume |
| x | $m$ | Height coordinate |
| Greek Symbols | | |
| $\alpha$ | $W/Km^2$ | Heat transfer coefficient |
| $\beta$ | $1/K$ | Volumetric thermal expansion coefficient |
| $\delta$ | $m$ | Wall thickness |
| $\theta$ | (-) | Semi-implicit parameter |
| $\lambda$ | $W/Km$ | Thermal Conductivity |
| $\nu$ | $m^2/s$ | Kinematic viscosity |
| $\rho$ | $kg/m^3$ | Density |
| $\tau$ | $s$ | Time constant |
| Subscripts | | |
| c | | property at the critical point |
| core | | Core property |
| in | | property at core inlet |
| pc | | Property at pseudo-critical point |
| Dimensionless numbers | | |
| DR | (-) | Decay ratio $e^{\frac{2\pi b_2}{abs\omega}}$ |
| $\mathrm{Gr}_L$ | (-) | Height-based Grashof number $Gr_L = \frac{g\beta(T_{wall}-T_{ambient})L^3}{\nu^2}$ |
| $\mathrm{Gr}_x$ | (-) | Local Grashof number $Gr_x = \frac{g\beta(T_{wall}-T_{ambient})x^3}{\nu^2}$ |
| Pr | (-) | Prandtl number $Pr = \frac{\nu\rho c_p}{\lambda}$ |
| $N_{SUB}$ | (-) | Subcooling number $N_{SUB} = \frac{h_{pc}-h_{in}}{h_{pc}}$ |
| $N_{PCH}$ | (-) | Pseudo phase change number $N_{PCH} = \frac{P_{core}}{Mh_{pc}}$ |
| $\mathrm{Nu}_L$ | (-) | Height-based average Nusselt Number $\frac{\alpha L}{\lambda}$ |

| | | |
|---|---|---|
| $\mathrm{Nu}_x$ | (-) | Local Nusselt Number $\frac{\alpha x}{\lambda}$ |

| Acronyms | |
|---|---|
| BWR | Boiling Water Reactor |
| DeLight | Delft Light Water Reactor |
| DWO | Density Wave Oscillation |
| LWR | Light Water Reactor |
| HPLWR | High Performance Light Water Reactor |
| NSB | Neutral Stability Boundary |
| SCWR | Super Critical Water Reactor |

# Appendix A

# Technical drawing of the DeLight facility

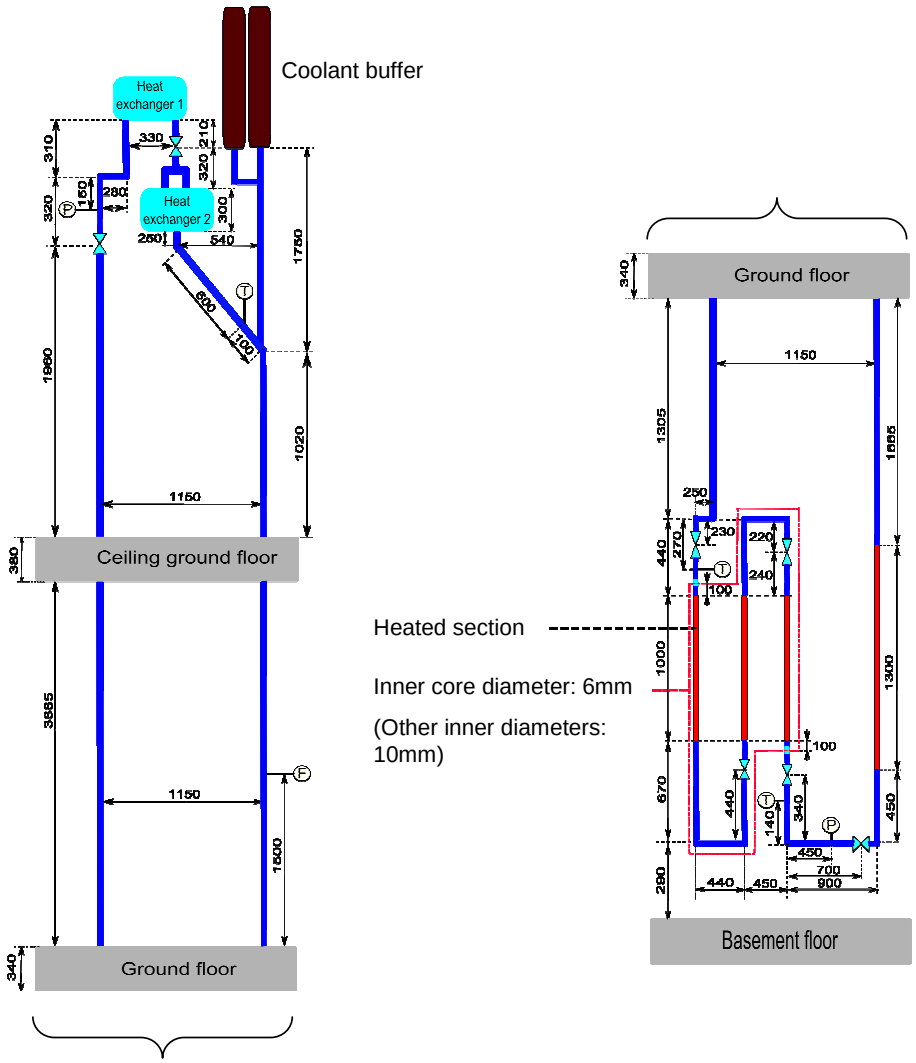


**Figure A.1:** Technical drawing of the DeLight facility. The heated sections are in red, the most right one is the preheater , the left three the evaporator and superheaters. Several sensors are indicated by letters: F - flow meter, T - thermocouple, P - absolute pressure sensor.

# Appendix B

# Flowchart of the numerical DeLight model

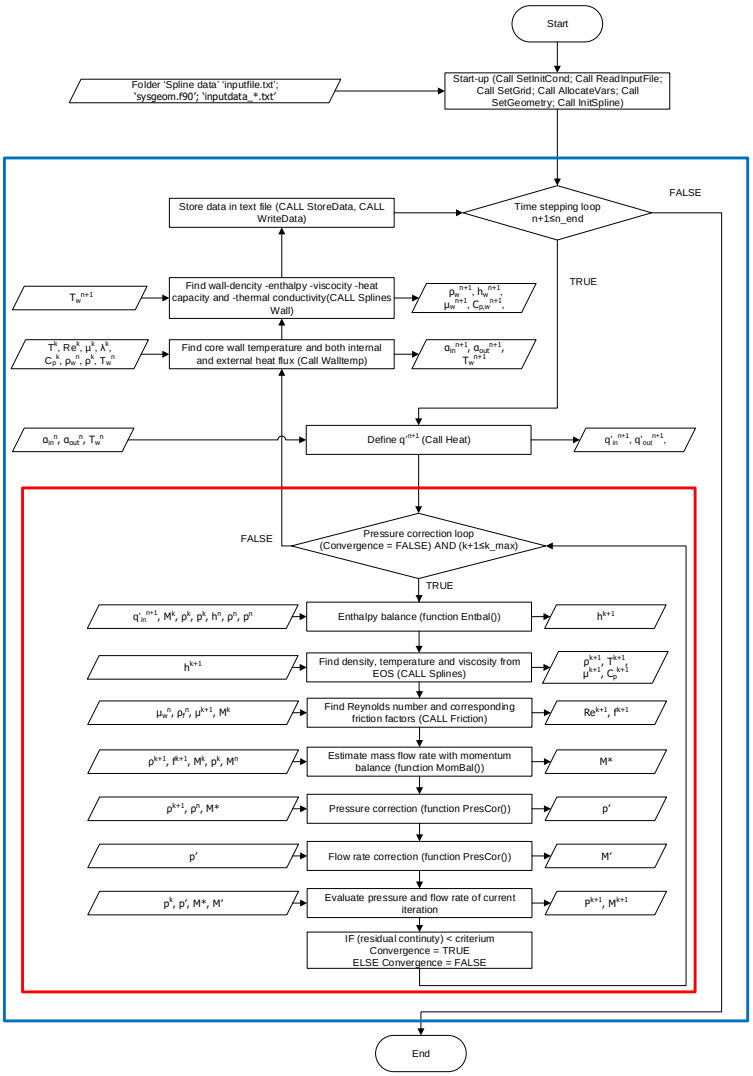


**Figure B.1:** Flowchart of the DeLight model. The boxes indicate two loops in the code. The blue box indicates the time step loop and the red box the pressure correction iteration.(Van Iersel, 2016)